septum was determined, and RV hypertrophy was expressed as RV weight/(left ventricle plus ventricular septum weights).[12,17]

The lungs were perfused with a solution of 10% phosphate-buffered formalin (pH 7.4). At the same time, 10% phosphate-buffered formalin (pH 7.4) was administered into the lungs via tracheal tube at a pressure of 20 cm H_2O. These specimens were processed for light microscopy by routine paraffin embedding. The degree of remodeling (muscularization) of small, peripheral, PAs was assessed by double immunohistochemical staining of the 5-μm sections with an anti–α-smooth muscle actin antibody (dilution 1:500; clone 1A4, Dako) and anti-platelet endothelial cell adhesion molecule-1 (PECAM-1) (M-20) antibody (dilution 1:100, Santa Cruz).[12] To assess the type of remodeling of muscular PAs, microscopic images were analyzed. In each rat, 30 to 40 intra-acinar arteries were categorized as muscular (those with a complete medial coat of muscle), partially muscular (those with only a crescent of muscle), or nonmuscular (those with no apparent muscle), counted, and averaged within a range of diameters from 25 to 50 μm.[12]

Histopathologic and Immunohistochemical Analysis of Rat Lungs

The degrees of monocyte infiltration were evaluated by immunostaining for ED-1 (analog of human CD68, Serotec). For quantification, a blinded observer counted the number of ED-1–positive cells in 10 fields. Sections were also subjected to immunostaining with antibodies against FITC (1:1000; American Research Products, Belmont, MA), an epitope (α-p65) on the p65 subunit of NF-κB (1:100; Boehringer Mannheim, Roche Diagnostics, Basel, Switzerland), rabbit eNOS (ABR: PA1–037), murine inducible NOS (iNOS, Transduction Laboratories), or nonimmune mouse IgG (Dako). The α-p65 monoclonal antibody recognizes an epitope on the p65 subunit that is masked by bound inhibitor-κB.[19] Therefore, this antibody exclusively detects activated NF-κB.[19]

Real-Time Quantitative Reverse Transcription–Polymerase Chain Reaction

Real-time polymerase chain reaction amplification was performed with rat cDNA with the use of an ABI PRISM 7000 sequence detection system (Applied Biosystems, Foster City, CA) as described previously.[12,19] TaqMan primers/probes for monocyte chemotactic protein-1, tumor necrosis factor-α, interleukin (IL)-1β, IL-6, intercellular adhesion molecule-1, and glyceraldehyde 3-phosphate dehydrogenase, which served as the endogenous reference, were purchased from Applied Biosystems (Assay-on-Demand gene expression products Rn00580555, Rn99999017, Rn00580432, Rn00561420, and Rn00564227 and TaqMan rodent glyceraldehyde 3-phosphate dehydrogenase control reagents, respectively).

Lipopolysaccharide-Induced Activation of Mouse Monocytes

The mouse macrophage cell line RAW 264.7 was purchased. After bacterial lipopolysaccharide (serotype 0111:B4, Sigma) at 1 μg/mL was added to the cells, each 1.0-mL suspension of pitavastatin at 5 mg/mL, FITC-NP (1 mg/mL PLGA), pitavastatin-NP containing 1.0 mg/mL PLGA and 5 mg/mL pitavastatin, or vehicle was added to the wells; 2 hours later, the cells were washed 3 times with PBS. NF-κB pathway activity was measured with a TransAM NF-κB p65 ELISA-based assay kit (Active Motif, Tokyo, Japan). Nuclear extracts of RAW 264.7 cells were prepared with the NE-PER nuclear and cytoplasmic extraction reagent kit (Pierce, Rockford, IL) according to the manufacture's protocol. Samples were placed, along with 30 μL of binding buffer, on a 96-well plate to which oligonucleotides containing an NF-κB consensus binding site had been immobilized for 1 hour on a shaker. During this time, the activated NF-κB contained in the sample specifically binds to this nucleotide; then the plate was washed and, by using a primary antibody (100 mL diluted 1:1000 in antibody binding buffer for 1 hour) that is directed against the NF-κB p65 subunit, the NF-κB complex bound to the oligonucleotides can be detected. The plate was then washed again, and 100 μL of secondary antibody (diluted 1:1000 in antibody binding buffer) conjugated to horseradish peroxidase was added for 1 hour. The plate was washed again, and 100 μL of developing solution was added. The plate was incubated for 4 minutes away from direct light, 100 μL of stop solution was added, and the plate was read with a plate reader at 450 nm.

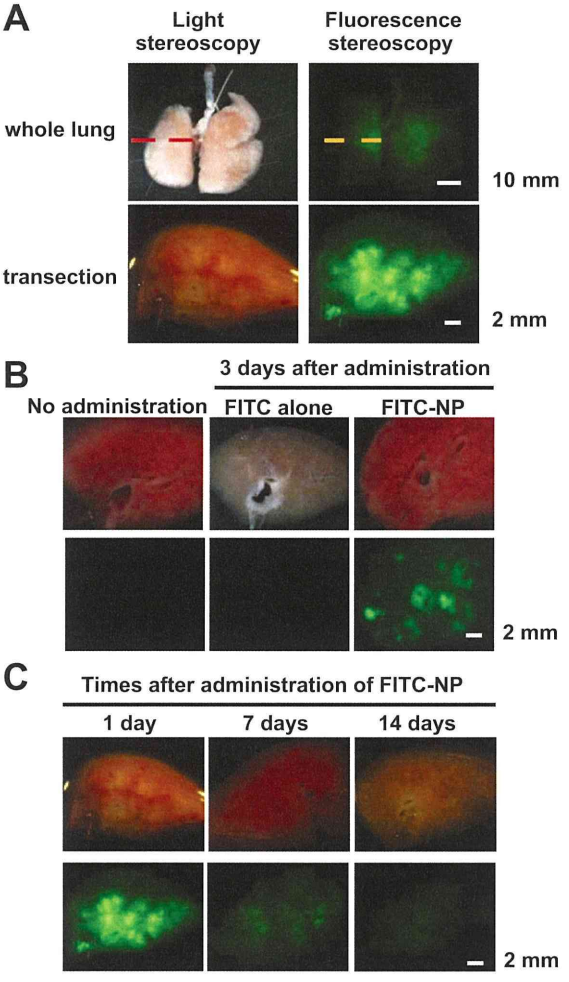

Figure 1. Localization of FITC-NP after instillation into the rat lung. A, Representative light (left) and fluorescence (right) stereomicrographs of whole lungs (upper) and transections (lower) 1 hour after intratracheal instillation of FITC-NP. B, Representative light (upper) and fluorescence (lower) stereomicrographs of transections from control (nontreated) lungs and from lungs instillated with FITC alone or FITC NP on day 3 after instillation. C, Representative light (upper) and fluorescence (lower) stereomicrographs of cross sections from lungs instillated with FITC-NP on days 1, 7, and 14 after instillation.

Western Blot Analysis

Protein was extracted from frozen lung tissues. Samples were homogenized in lysis buffer containing 10 mmol/L Tris-HCl, pH 7.4, 50 mmol/L NaCl, 5 mmol/L EDTA, 1% Triton X-100, 50 mmol/L NaCl, 30 mmol/L sodium phosphate, 50 mmol/L NaF, 1% aprotinin, 0.5% pepstatin A, 2 mmol/L phenylmethylsulfonyl fluoride, and 5 mmol/L leupeptin and phosphatase inhibitor cocktail (Pierce). Cell lysates (50 μg) were separated on 7.5% polyacrylamide gels and blotted onto polyvinylidene difluoride membranes (Millipore Co, Hercules, CA). Protein expression was analyzed by using antibodies against eNOS (ABR: PA1–037) or actin (Sigma). Immune complexes were visualized with horseradish peroxidase–conjugated secondary antibodies. Bound antibodies were detected by chemiluminescence with the use of an ECL detection system (Amersham Biosciences) and quantified by densitometry.

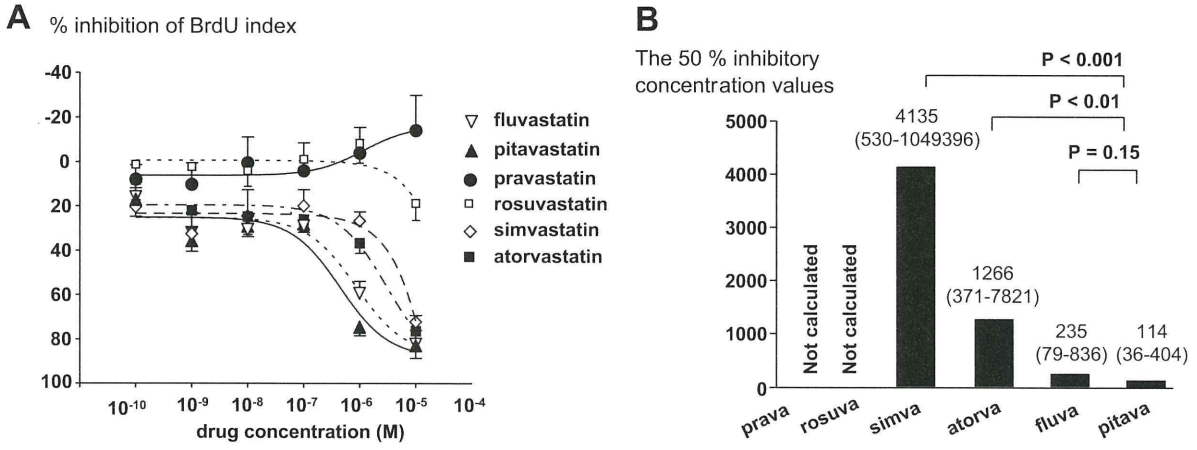

Figure 2. Inhibitory effects of various statins on human PASMC proliferation. A, PASMC proliferation assay (% inhibition of 5′-bromo-2′-deoxyuridine [BrdU] index) in response to various concentrations of various statins (n=6 per group). B, IC_{50} values and 95% Wald CIs (in parentheses) are shown at the top of each bar. Probability values vs pitavastatin by Wald tests in a 4-parameter logistic-regression model are shown. Prava indicates pravastatin; rosuva, rosuvastatin; simva, simvastatin; atorva, atorvastatin; fluva, fluvastatin; and pitava, pitavastatin.

Measurements of Pitavastatin Concentration

Pitavastatin concentrations in serum and lung were measured at predetermined time points by using a column-switching high-performance liquid chromatography system, as previously reported.[20] In brief, the column-switching high-performance liquid chromatography system consists of 2 LC-10AD pumps, an SIL-10A autosampler, a CTO-10A column oven, a 6-port column-switching valve, and an SPD-10A UV detector (all from Shimadzu, Kyoto, Japan). The column temperature was maintained at 40°C. Preprepared serum or tissue homogenate sample solutions were injected from the autosampler into the high-performance liquid chromatography system, and detection of the statin in sample solutions was performed at 250 nm with a UV detector. The detected peak area was measured with Lcsolution software (Shimadzu).

Statistical Analysis

Data are presented as mean±SEM. Statistical analysis of differences was performed by 1-way ANOVA and Bonferroni's multiple comparison tests. The survival rates were determined by the Kaplan-Meier method. Efficacy ratios (median inhibitory concentration [IC_{50}]values) of statins were tested with Wald tests in a 4-parameter logistic-regression model. Point estimates and Wald 95% CIs for IC_{50} values were calculated. Statistical calculations were performed with SAS preclinical package software version 9.1.3 (SAS Institute Inc, Tokyo, Japan) and Prism Software version 4.0.1 (GrafPad). A value of $P<0.05$ was considered statistically significant.

Results

Localization of FITC-NP in the Lung of Rats With MCT-Induced PAH

Localization of FITC was examined after a single intratracheal instillation of FITC-NP into animals injected with MCT. Three days after instillation, strong FITC signals were detected only in FITC-NP–instillated lungs, whereas no or only faint FITC signals were observed in control noninjected lungs and in lungs injected with FITC only (Figure 1). On days 1, 7, and 14, FITC signals remained localized predominantly in the lungs. There were FITC-positive cells in the bronchi and alveoli, alveolar macrophages, and small arteries. As we previously reported,[12] immunofluorescence staining revealed that FITC signals localized mainly in small arteries and arterioles as well as in small bronchi and alveoli 14 days after instillation of FITC-NP (online-only Figure I). FITC signals were not detected in remote organs (liver, spleen, and heart) at any time point (data not shown).

Inhibitory Effects of Statins on Human PASMC Proliferation

To implicate pitavastatin as a candidate statin for nanoparticulation, the effects of statins on PASMC proliferation were examined. In a human PASMC proliferation assay (percent inhibition of 5′-bromo-2′-deoxyuridine index), hydrophilic statins (rosuvastatin and pravastatin) elicited no inhibitory effects, whereas other statins showed dose-dependent effects (Figure 2A). The IC_{50} value of pitavastatin was lower than that of simvastatin or atorvastatin (Figure 2B). The IC_{50} value of pitavastatin tended to be lower than that of fluvastatin, but there was no significant difference in the IC_{50} values between the 2 statins.

Effects of Pitavastatin-NP on the Development of PAH in the Rat Model of MCT-Induced PAH

An RV catheterization study confirmed that injection of MCT led to severe PAH (increased RV systolic pressure) associated with small PA remodeling and increased infiltration of ED1-positive monocytes 3 weeks after MCT injection, as previously reported.[12,17] Single intratracheal treatment with pitavastatin-NP, but not with pitavastatin alone or FITC-NP, attenuated the development of PAH, small PA remodeling, and monocyte-mediated inflammation (Figure 3). The RV systolic pressure of untreated normal controls (no MCT injection) was 34±2 mm Hg (n=10). There were no significant differences in concentrations of pitavastatin in the lung and systemic blood between pitavastatin-NP–treated and pitavastatin-only groups (the Table).

Echocardiographic study showed that there were no significant changes in cardiac output or stroke volume among untreated control and MCT-induced PAH rats (online-only Table I). Echo-derived estimation of RV systolic pressure and pulmonary vascular resistance showed the development of MCT-induced PAH and therapeutic effects of a single intra-

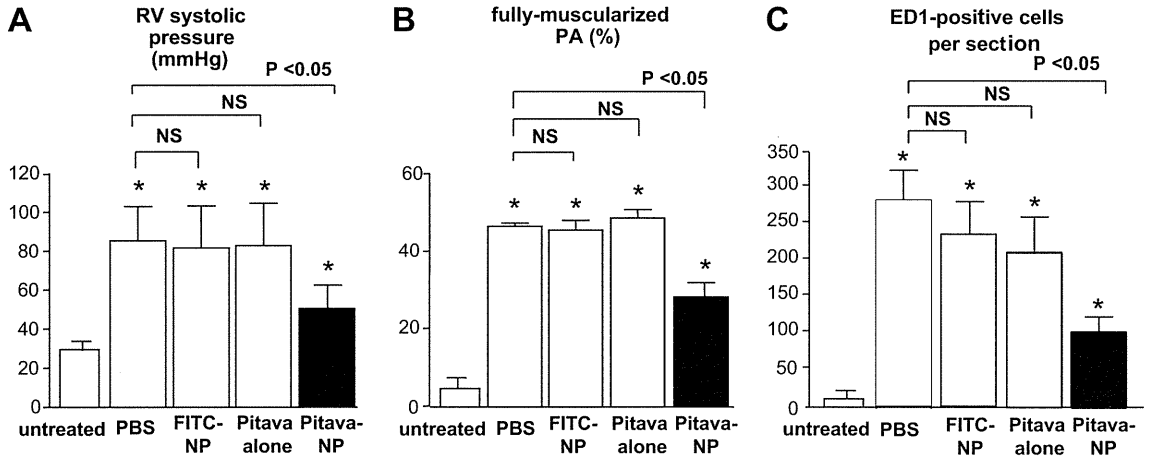

Figure 3. Effects of pitavastatin (pitava)-NP on RV systolic pressure, small PA remodeling, and infiltration of monocytes 3 weeks after MCT injection. A, RV systolic pressure in the 4 experimental groups. Data are mean±SEM (n=6 per group). B, Percentage of fully muscularized small PAs in the 4 experimental groups. Data are mean±SEM (n=6 per group). C, Infiltration of ED1-positive monocytes into the lung (the number of positive cells per 30 high-power-field cross sections). Data are mean±SEM (n=6 per group). *P<0.01 vs untreated control.

tracheal instillation of pitavastatin-NP, as reported by the RV catheterization study.

The activity of lactate dehydrogenase was not detected in bronchoalveolar lavage fluid. There were no significant changes in activity of lactate dehydrogenase and various biomarkers in lung tissue homogenates among untreated control and MCT-induced PAH rats (online-only Tables II and III).

Oral daily administration of pitavastatin at 0.3 mg/kg had no significant effects on MCT-induced PAH, but pitavastatin at 1.0, 3.0, and 10 mg/kg significantly attenuated the development of PAH (online-only Figure II).

Effects of Intratracheal Instillation of Pitavastatin-NP on NF-κB Activation and PAMSC Proliferation

As previously reported,[12] immunohistochemically detectable NF-κB activation was noted mainly in alveolar macrophages and weakly in PA lesions 7 days after MCT administration (Figure 4). A single intratracheal instillation of pitavastatin-NP, but not of FITC-NP or pitavastatin alone, markedly attenuated the increases in NF-κB (α-p65) activity induced by MCT injection (Figure 4). Because NF-κB was activated in alveolar monocytes in MCT-induced PAH, effects of pitavastatin-NP on NF-κB activity were examined in a monocyte cell line (RAW 264.7 cells) in vitro. Treatment with pitavastatin-NP, but not with pitavastatin only, attenuated NF-κB activation in RAW 264.7 cells (online-only Figure III). Because proliferation of PASMCs is increased in animals and humans with PAH, effects of pitavastatin and pitavastatin-NP were examined in human PASMCs in vitro. Treatment with pitavastatin-NP, but not with pitavastatin only, attenuated the proliferation of PASMCs (online-only Figure IV).

Table. Pitavastatin Concentrations in the Lung and Systemic Blood After Intratracheal Administration of Pitavastatin (100 μg per Animal) Only or Pitavastatin-NP Containing the Same Dose of Pitavastatin

	Time After Administration, h					
Groups	1	3	6	12	24	48
Pitavastatin-only group						
Lung, ng/g	115±83	49±69	7±5	2±1	3±3	4±3
Serum, ng/mL	48±19	24±10	9±7	1±1	1±1	1±1
Pitavastatin-NP group						
Lung, ng/g	155±77	17±8	13±13	4±6	7±4	3±1
Serum, ng/mL	65±19	20±5	7±4	2±1	1±1	1±2

Data are mean±SEM (n=6 per group).

Effects of Pitavastatin-NP on Expression of Proinflammatory Factors

As previously reported,[12] MCT-induced PAH was associated with increased gene expression of proinflammatory factors. Intratracheal treatment with pitavastatin-NP significantly reduced the increased gene expression of monocyte chemotactic protein-1, tumor necrosis factor-α, and IL-6 and tended to decrease the expression of IL-1β and intercellular adhesion molecule-1 (online-only Figure V).

Effects of Pitavastatin-NP on eNOS and iNOS Expression

Because the protective effects of statins on PAH have been reported to be attributable at least to the eNOS-related pathway,[11] eNOS protein expression in the lungs was examined on days 3 and 21 after treatment. Western blot analysis showed that MCT administration had no significant effect on eNOS expression on days 3 and 21, compared with untreated controls (Figure 5). Pitavastatin-NP, but not FITC-NP or pitavastatin alone, increased the protein expression of eNOS on day 3, whereas pitavastatin-NP showed no therapeutic effects on eNOS expression on day 21 (Figure 5).

In contrast, iNOS is known to cause oxidant tissue injury and accelerates the pathologic processes of PAH.[21] Immuno-

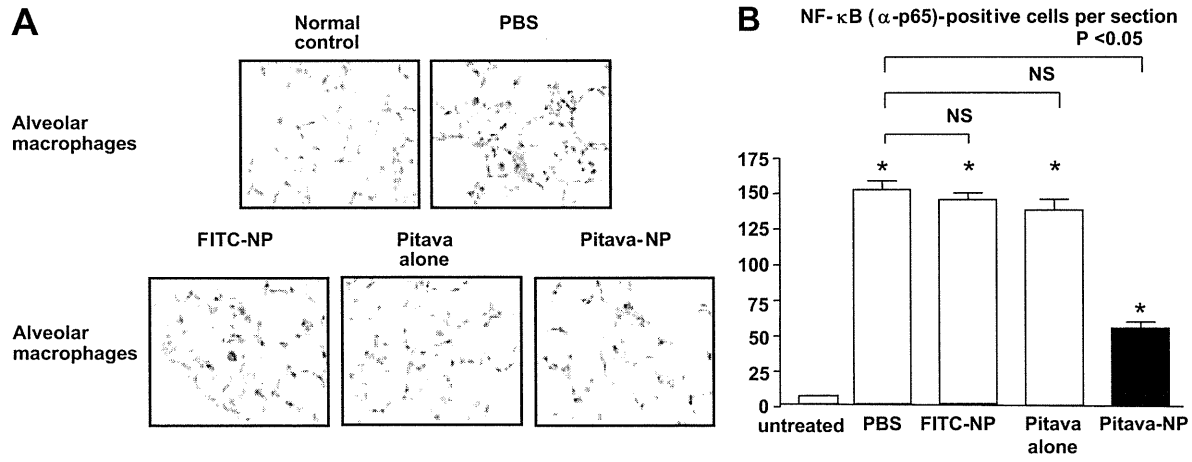

Figure 4. Effects of pitavastatin (pitava)-NP on NF-κB activation. A, Photomicrographs of cross sections of lung stained immunohistochemically with NF-κB (α-p65) from normal rats and PAH rats 3 days after MCT injection. B, Effects of pitavastatin-NP on infiltration of NF-κB (α-p65)–positive cells 3 days after MCT injection. Data are mean±SEM (n=6 per group). *$P<0.01$ vs untreated control.

histochemical expression of iNOS was not detected in lung sections from untreated control rats. Immunostaining for iNOS was noted mainly in alveolar macrophage and weakly in PA lesions 3 days after MCT administration (online-only Figure VI). Single intratracheal instillation of pitavastatin-NP, but not of FITC-NP or pitavastatin only, markedly attenuated the increase in iNOS activity induced by MCT injection.

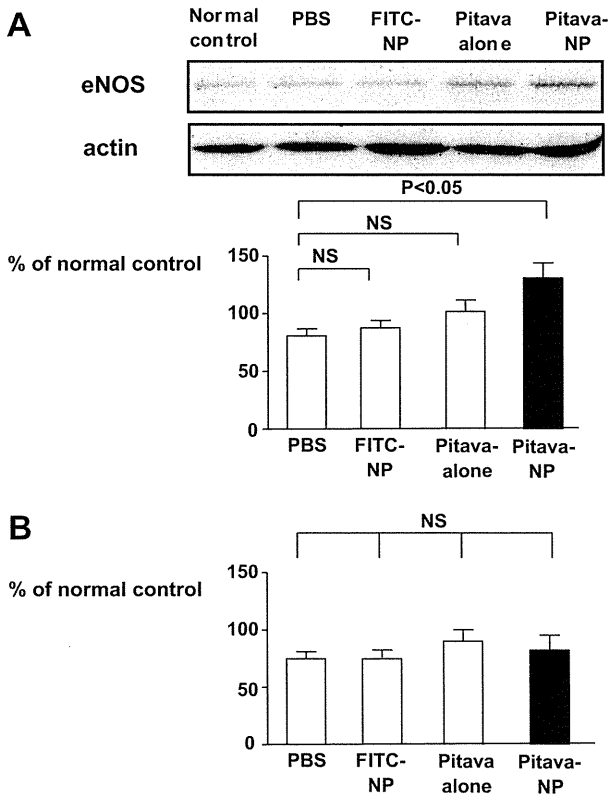

Figure 5. Effects of pitavastatin (pitava)-NP on eNOS protein expression. A, eNOS expression in the lung 3 days after MCT injection. The eNOS level is shown as a percentage of the internal-control actin level. n=6 per group. B, eNOS expression in the lung 21 days after MCT injection. The eNOS level is shown as a percentage of the internal-control actin level. n=6 per group.

Effects of Pitavastatin-NP on Survival

In the treatment protocol, pitavastatin-NP significantly improved survival rate: 42% in the PBS group (n=40), 39% in the FITC-NP group (n=33), 40% in the pitavastatin-alone group (n=40), and 64% in the pitavastatin-NP group (n=58; Figure 6). In addition, pitavastatin-NP caused regression of MCT-induced PAH (Figure 6).

Discussion

We recently reported that intratracheal instillation of a polyethylene glycol-*block*-PLGA copolymer (PEG-PLGA) is an excellent system for drug delivery to the lung.[12] We found in the present study that PLGA NPs were as effective as PEG-PLGA NPs as an NP-mediated drug delivery system to the lung. As we reported with PEG-PLGA NPs,[12] the FITC signals were detected in small bronchial tracts, alveolar macrophages, and small PAs for up to 14 days after a single instillation of FITC-encapsulated PLGA NP.

Statins are known to ameliorate the effects of endothelial injury/dysfunction by enhancing the activity of eNOS and thus, exert multiple vasculoprotective effects on other cell types (vascular smooth muscle cells, monocytes, etc).[3–5] We recently reported that NP-mediated pitavastatin delivery to the vascular endothelium of ischemic skeletal muscles effectively increased therapeutic neovascularization in a murine model of hindlimb ischemia.[13] In our previous study, the beneficial effects of pitavastatin-NP were mediated by increased activity of eNOS.[13] Notably, NP-mediated delivery of pitavastatin had greater angiogenic activity in human endothelial cells in vitro compared with pitavastatin alone.[13] We therefore hypothesized that eNOS and downstream pathogenetic factors might be involved in the therapeutic effects of NP-mediated pitavastatin delivery on MCT-induced PAH. Among statins, pitavastatin was selected as the nanoparticulation compound because this drug elicited the most potent angiogenic effects in human endothelial cells[14] and the most

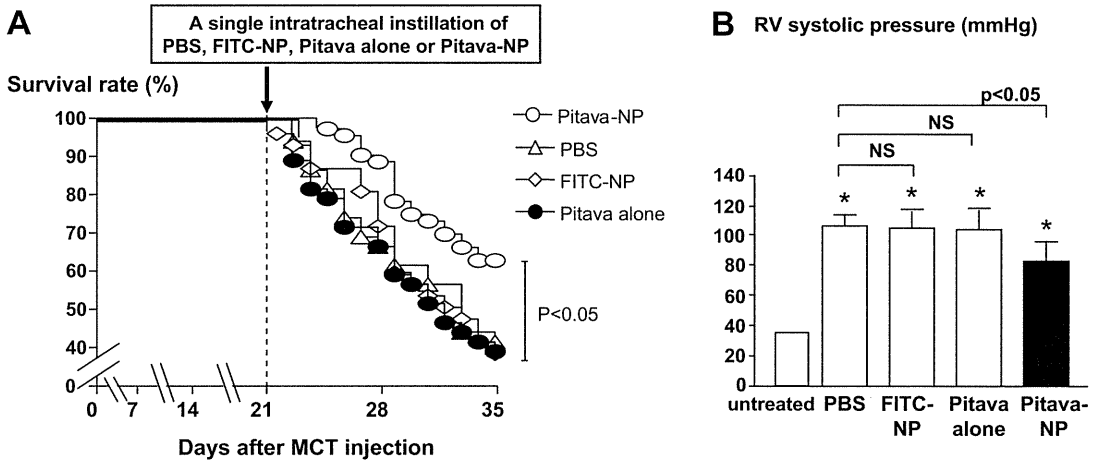

Figure 6. Effects of pitavastatin (pitava)-NP on RV systolic pressure and survival rate. A, Survival curves analyzed by the Kaplan-Meier method in PBS, FITC-NP, pitavastatin only, and pitavastatin-NP groups. B, RV systolic pressure (in mm Hg) in the 4 experimental groups 2 weeks after treatment (at week 5 after MCT injection).

potent inhibitory effects on human PASMC proliferation (Figure 2) in vitro compared with other statins. We also found that NP-mediated intracellular delivery of pitavastatin showed greater inhibitory effects on PASMC proliferation and on NF-κB activation in a monocyte cell line (RAW 264.7 cells) compared with pitavastatin alone (online-only Figures III and IV). Collectively, these in vitro data suggest that NP-mediated pitavastatin delivery is more effective than pitavastatin in inhibiting PASMC proliferation and monocyte activation and improving the deleterious effects of endothelial injury/dysfunction.

The important novel finding of the present study is that a single intratracheal instillation of pitavastatin-NP attenuated the development of PAH (increased RV pressure, PA resistance, and PA remodeling) associated with reduced activity of NF-κB and NF-κB–dependent inflammatory factors (for example, monocyte chemotactic protein-1, IL-1, tumor necrosis factor-α, iNOS, etc). In contrast, eNOS expression was not reduced in the PBS group but was increased by day 3 only but not by day21 (Figure 5), suggesting that eNOS plays a minor role in the therapeutic effects of pitavastatin-NP. Intratracheal instillation of pitavastatin alone at the same dose had no therapeutic effect. Concentrations of pitavastatin in the lungs and systemic blood were found to be similar between animals treated with pitavastatin-NP and those treated with pitavastatin only (the Table). These findings suggest a specific advantage of NP-mediated delivery of pitavastatin to induce therapeutic effects. Therefore, the beneficial effects of pitavastatin-NP on MCT-induced PAH in vivo can be attributable to the pleiotropic effects of pitavastatin-NP, including inhibition of inflammation and cell proliferation.

Prior studies have reported that daily oral administration of statins at high doses beyond the clinical norm (a regimen that could lead to serious adverse side effects in a clinical setting) attenuates MCT- and hypoxia-induced PAH in animals.[7–9] We thus examined whether NP-mediated pitavastatin delivery would be superior to daily oral administration of pitavastatin alone in inhibiting MCT-induced PAH, and we found that oral daily administration of pitavastatin at 0.3 mg/kg per day for 21 days (cumulative dose=25.2 mg per animal, assuming the body weight of animals to be 250 g) had no therapeutic effects, but the same regimen of pitavastatin at 1, 3, and 10 mg/kg per day (cumulative doses=84, 252, and 840 mg per animal, respectively) did show significant therapeutic effects. Therefore, our NP-mediated delivery system (single injection of 0.1 mg pitavastatin per animal) seems to be as effective at an ≈840-times lower dose than the cumulative systemic dose.

It is noteworthy that a single intratracheal treatment with pitavastatin-NP 3 weeks after MCT injection induced regression of PAH and improved survival rate. This finding is more clinically significant than is the mere prevention of PAH. These results suggest that this NP-mediated delivery of pitavastatin may have beneficial therapeutic effects in patients with established PAH.

Perspectives

This mode of NP-mediated delivery of pitavastatin into the lungs is more effective in attenuating the development of MCT-induced PAH compared with intratracheal treatment with pitavastatin alone or systemic administration of pitavastatin, and treatment with pitavastatin-NP induced regression of established PAH. For translation of our present findings into clinical medicine, more clinical studies are needed to investigate whether pitavastatin-NP by inhalation might be effective in improving PAH.

Source of Funding

This study was supported by Health Science Research grants (Research on Nano-medicine and on Intractable Diseases) from the Ministry of Health Labor and Welfare, Tokyo, Japan.

Disclosures

Dr Egashira holds a patent on the results reported in this study. The remaining authors report no conflicts of interest.

References

1. Farber HW, Loscalzo J. Pulmonary arterial hypertension. *N Engl J Med.* 2004;351:1655–1665.
2. Humbert M, Sitbon O, Simonneau G. Treatment of pulmonary arterial hypertension. *N Engl J Med.* 2004;351:1425–1436.

3. Takemoto M, Liao JK. Pleiotropic effects of 3-hydroxy-3-methylglutaryl coenzyme A reductase inhibitors. *Arterioscler Thromb Vasc Biol.* 2001; 21:1712–1719.
4. Egashira K, Hirooka Y, Kai H, Sugimachi M, Suzuki S, Inou T, Takeshita A. Reduction in serum cholesterol with pravastatin improves endothelium-dependent coronary vasomotion in patients with hypercholesterolemia. *Circulation.* 1994;89:2519–2524.
5. Egashira K. Clinical importance of endothelial function in arteriosclerosis and ischemic heart disease. *Circ J.* 2002;66:529–533.
6. Ni W, Egashira K, Kataoka C, Kitamoto S, Koyanagi M, Inoue S, Takeshita A. Anti-inflammatory and antiarteriosclerotic actions of HMG-CoA reductase inhibitors in a rat model of chronic inhibition of nitric oxide synthesis. *Circ Res.* 2001;89:415–421.
7. Girgis RE, Mozammel S, Champion HC, Li D, Peng X, Shimoda L, Tuder RM, Johns RA, Hassoun PM. Regression of chronic hypoxic pulmonary hypertension by simvastatin. *Am J Physiol.* 2007;292: L1105–L1110.
8. Nishimura T, Faul JL, Berry GJ, Vaszar LT, Qiu D, Pearl RG, Kao PN. Simvastatin attenuates smooth muscle neointimal proliferation and pulmonary hypertension in rats. *Am J Respir Crit Care Med.* 2002;166: 1403–1408.
9. Nishimura T, Vaszar LT, Faul JL, Zhao G, Berry GJ, Shi L, Qiu D, Benson G, Pearl RG, Kao PN. Simvastatin rescues rats from fatal pulmonary hypertension by inducing apoptosis of neointimal smooth muscle cells. *Circulation.* 2003;108:1640–1645.
10. McMurtry MS, Bonnet S, Michelakis ED, Bonnet S, Haromy A, Archer SL. Statin therapy, alone or with rapamycin, does not reverse monocrotaline pulmonary arterial hypertension: the rapamycin-atorvastatin-simvastatin study. *Am J Physiol.* 2007;293:L933–L940.
11. Rhodes CJ, Davidson A, Gibbs JS, Wharton J, Wilkins MR. Therapeutic targets in pulmonary arterial hypertension. *Pharmacol Ther.* 2009;121: 69–88.
12. Kimura S, Egashira K, Chen L, Nakano K, Iwata E, Miyagawa M, Tsujimoto H, Hara K, Morishita R, Sueishi K, Tominaga R, Sunagawa K. Nanoparticle-mediated delivery of nuclear factor-κB decoy into lungs ameliorates monocrotaline-induced pulmonary arterial hypertension. *Hypertension.* 2009;53:877–883.
13. Kubo M, Egashira K, Inoue T, Koga J, Oda S, Chen L, Nakano K, Matoba T, Kawashima Y, Hara K, Tsujimoto H, Sueishi K, Tominaga R, Sunagawa K. Therapeutic neovascularization by nanotechnology-mediated cell-selective delivery of pitavastatin into the vascular endothelium. *Arterioscler Thromb Vasc Biol.* 2009;29:796–801.
14. Oda S, Nagahama R, Nakano K, Matoba T, Kubo M, Sunagawa K, Tominaga R, Egashira K. Nanoparticle-mediated endothelial cell-selective delivery of pitavastatin induces functional collateral arteries (therapeutic arteriogenesis) in a rabbit model of chronic hind limb ischemia. *J Vasc Surg.* 2010;52:412–420.
15. Kawashima Y, Yamamoto H, Takeuchi H, Hino T, Niwa T. Properties of a peptide containing DL-lactide/glycolide copolymer nanospheres prepared by novel emulsion solvent diffusion methods. *Eur J Pharm Biopharm.* 1998;45:41–48.
16. Kawashima Y, Yamamoto H, Takeuchi H, Fujioka S, Hino T. Pulmonary delivery of insulin with nebulized DL-lactide/glycolide copolymer (PLGA) nanospheres to prolong hypoglycemic effect. *J Control Release.* 1999;62:279–287.
17. Ikeda Y, Yonemitsu Y, Kataoka C, Kitamoto S, Yamaoka T, Nishida K, Takeshita A, Egashira K, Sueishi K. Anti-monocyte chemoattractant protein-1 gene therapy attenuates pulmonary hypertension in rats. *Am J Physiol Heart Circ Physiol.* 2002;283:H2021–H2028.
18. Urboniene D, Haber I, Fang YH, Thenappan T, Archer SL. Validation of high-resolution echocardiography and magnetic resonance imaging versus high-fidelity catheterization in experimental pulmonary hypertension. *A J Physiol.* 2010;299:401–412.
19. Ohtani K, Egashira K, Nakano K, Zhao G, Funakoshi K, Ihara Y, Kimura S, Tominaga R, Morishita R, Sunagawa K. Stent-based local delivery of nuclear factor-κB decoy attenuates in-stent restenosis in hypercholesterolemic rabbits. *Circulation.* 2006;114:2773–2779.
20. Kojima J, Fujino H, Yosimura M, Morikawa H, Kimata H. Simultaneous determination of NK-104 and its lactone in biological samples by column-switching high-performance liquid chromatography with ultraviolet detection. *J Chromatogr.* 1999;724:173–180.
21. Hampl V, Bibova J, Banasova A, Uhlik J, Mikova D, Hnilickova O, Lachmanova V, Herget J. Pulmonary vascular iNOS induction participates in the onset of chronic hypoxic pulmonary hypertension. *Am J Physiol.* 2006;290:L11–L20.

ONLINE SUPPLEMENT

Nanoparticle-Mediated Delivery of Pitavastatin into Lungs Ameliorates Development and Induces Regression of Monocrotaline-induced Pulmonary Arterial Hypertension

Ling Chen, Kaku Nakano, Satoshi Kimura, Tetsuya Matoba, Eiko Iwata, Miho Miyagawa, Hiroyuki Tsujimoto, Kazuhiro Nagaoka, Junji Kishimoto, Kenji Sunagawa, Kensuke Egashira

Department of Cardiovascular Medicine (LC, KN, TM, EI, MM, KN, KS, KE) and Digital Medicine Initiative (JK), Graduate School of Medical Science, Kyushu University, Fukuoka, Japan; and Hosokawa Micron Corporation (HT), Osaka, Japan.

Address for correspondence:
Kensuke Egashira, M.D. Ph.D.
Department of Cardiovascular Medicine
Graduate School of Medical Science, Kyushu University
3-1-1, Maidashi, Higashi-ku,
Fukuoka 812-8582, Japan
Phone : +81-92-642-5358
Fax : +81-92-642-5375
E-mail: egashira@cardiol.med.kyushu-u.ac.jp

Materials and Methods

Echocardiographic measurements of RV and PA hemodynamics

Transthoracic 2-D, M-mode and pulsed-wave Doppler Echo were obtained with a 30 MHz transducer (Vevo 2100 ultrasound system; Primetech Inc). [1] M-mode and 2-D modalities were applied to measure RV free wall thickness during end diastole and RV wall stress. These images were obtained from the right side of the rat, with the ultrasonic beam positioned perpendicularly to the wall of the midthird of the RV.

PA diameter was measured at the level of pulmonary outflow tract during midsystole using the superior angulation of the parasternal short-axis view. M-mode measurements were performed from "leading edge to leading edge" (epicardial to endocardial) as recommended by the American Society of Echocardiography.

Pulsed-wave Doppler was used to measure PA acceleration time (PAAT) and PA flow velocity time integral. The Doppler sample volume was centrally positioned within the main PA, just distal from the pulmonary valve with the beam oriented parallel to the flow. The sweep speed for the Doppler flow recordings was 400–800 mm/s. RV ejection time was measured as the interval from the onset to the end of ejection in milliseconds. Thereafter, pulmonary artery acceleration time normalized for cycle length, RV systolic pressure, and pulmonary vascular resistance (PVR) were estimated. Stroke volume (SV), CO, and cardiac index (CI) were also calculated.

Measurement of lactate dehydrogenase To examine cytotoxicity of intratracheal treatment of pitavastatin-NP, the activity of lactate dehydrogenase (LDH) in bronchoalveolar lavage fluid (BALF) and lung tissue homogenates was measured 7 days after MCT administration using an assay kit LDH (Wako Pure Chemical Industries, Ltd.) according to the manufacturer's instructions in separate series of experiments.

Measurement of biomarkers by multiplex immunoassay Tissue concentrations of various biomarkers in ling tissue homogenates were measured 7 days after MCT administration using the Luminex LabMAP instruments (Table III), which was ordered to biomarker analysis services of Charles River Inc (http://www.criver.com/en-US/ProdServ/ByType/Discovery/Pages/PlasmaBiomarkerAnalysis.aspx).

1. Urboniene D, Haber I, Fang YH, Thenappan T, Archer SL. Validation of High-Resolution Echocardiography and Magnetic Resonance Imaging Versus High-Fidelity Catheterization in Experimental Pulmonary Hypertension. *Am J Physiol Lung Cell Mol Physiol.*

Table S1. Echocardiographic characteristics of untreated control and MCT-induced PAH rats in prevention study

		MCT-induced PAH			
parameters	untreated control	PBS	FITC NP	Pitava alone	Pitava-NP
Cardiac output (mL/min)	120 ± 17	97 ±21	104 ±20	102 ±20	113 ±16
Stroke volume (mL)	0.29±0.04	0.24±0.05	0.26±0.06	0.26±0.05	0.28±0.05
Heart rate (beats per minute)	412 ± 26	408 ±36	399 ±39	397 ±32	405 ±25
PAAT/cl (x 100)	18 ±1	7 ±1*	7 ±1*	7 ±1*	12 ±1*†
eRVSP (mmHg)	20 ±3	65 ±11*	66 ±9*	62 ±7*	41 ±5 *†
PVR (mmHg/ml/min)	0.12 ±0.02	0.46 ±0.20*	0.43 ±0.12*	0.40 ±0.01*	0.24 ±0.05*†
RV wall thickness (mm)	0.64 ±0.05*	1.16 ±0.14*	1.05 ±0.10*	0.97 ± 0.06*	0.88 ±0.09*†
RV wall stress	20 ±5	48 ±19*	56 ± 26*	48 ±12*	24 ±8†

Data are the mean± SEM (n=6 each).
*P< 0.05 versus untreated control group
† P< 0.05 versus PBS group.
Abbreviations: PAAT/cl = normalized pulmonary artery acceleration time; eRVSP = estimated RV systolic pressure; PVR = pulmonary vascular resistance.

Table S2. Lactate dehydrogenase activity in cell-free bronchial lavage fluid and lung tissue homogenates 7 days after monocrotaline administration

		monocrotaline			
Sample sites	Untreated control	PBS group	FITC NP group	Pitava alone group	Pitava NP group
bronchial lavage fluid (IU/mL)	ND	ND	ND	ND	ND
Lung tissue (IU/ng protein)	8.6±3.4	2.8±1.1	10.9±6.0	5.7±4.6	11.8±4.9

Data are the mean± SEM (n=6 each). ND = not detected (under limit of detection).
There is no significant difference (P=0.56) among 5 groups by one-way ANOVA.

Table S3. Cytokines and other proteins in lung tissue homogenates 7 days after monocrotaline administration

parameters	unit	Untreated control	PBS group	FITC NP group	Pitava alone group	Pitava NP group
Apo A1	μg/mg	0.14±0.05	0.10±0.03	0.09±0.01	0.10±0.01	0.10±0.01
CD40	pg/mg	N.D.	N.D.	N.D.	N.D.	N.D.
CD40 Ligand	pg/mg	43±16	34±14	25±3	30±8	39±13
CRP	μg/mg	1.3±0.3	1.2±0.2	1.3±0.4	1.3±0.2	1.6±0.2
ET-1	pg/mg	61±36	67±29	61±18	64±15	56±15
Eotaxin	pg/mg	49±12	53±15	40±8	45±17	63±11
EGF mouse	pg/mg	0.54±0.21	0.55±0.21	0.40±0.08	0.44±0.09	0.44±0.07
Factor VII	ng/mg	0.53±0.12	0.58±0.17	0.47±0.07	0.48±0.07	0.53±0.08
FGF-9	ng/mg	0.10±0.02	0.09±0.03	0.07±0.01	0.08±0.01	0.08±0.03
FGF-basic	ng/mg	0.21±0.04	0.21±0.06	0.17±0.04	0.22±0.04	0.24±0.04
GCP-2 Rat	pg/mg	6.5±1.6	7.4±3.2	6.7±1.3	8.1±1.0	7.6±7
GM-CSF	pg/mg	N.D.	N.D.	N.D.	N.D.	N.D.
Haptoglobin	μg/mg	0.80±0.30	1.13±0.40	1.04±0.26	1.19±0.12	1.18±0.25
IFN-gamma	pg/mg	0.12±0.06	0.24±0.09	0.23±0.10	0.18±0.07	0.18±0.05
IP-10	pg/mg	1.7±0.3	2.2±1.0	1.7±0.3	1.7±0.5	2.1±0.8
IL-1 alpha	pg/mg	5.3±4.8	9.7±7.1	4.6±1.0	7.8±2.9	5.7±3.3
IL-1 beta	ng/mg	N.D.	N.D.	N.D.	N.D.	N.D.
IL-10	pg/mg	3.1±1.5	2.5±1.5	1.4±0.8	1.8±0.3	1.9±0.9
IL-11	pg/mg	9.8±5.6	6.1±1.6	6..1±4.8	5.9±1.0	6.8±2.0
IL-12p70	pg/mg	1.5±0.4	1.3±0.4	1.2±0.4	1.0±0.1	1.2±0.4
IL-17A	pg/mg	0.2±0.04	0.2±0.09	0.2±0.05	0.2±0.05	0.2±0.02
IL-18	ng/mg	0.2±0.1	0.2±0.1	0.2±0.1	0.2±0.0	0.2±0.1
IL-2	pg/mg	1.7±0.7	1.4±1.1	0.6±0.3	0.8±0.6	0.9±0.7
IL-3	pg/mg	1.1±0.5	0.9±0.3	0.9±0.4	0.7±0.3	0.8±0.2
IL-4	pg/mg	N.D.	N.D.	N.D.	N.D.	N.D.
IL-5	ng/mg	N.D.	N.D.	N.D.	N.D.	N.D.
IL-6	pg/mg	N.D.	N.D.	N.D.	N.D.	N.D.
IL-7	pg/mg	3.9±0.7	3.5±2.0	3.4±0.8	3.0±0.3	3.2±0.6
LIF	pg/mg	33.9±9.8	38.3±12.5	29.9±4.3	31.6±4.1	35.7±6.1
Lymphotactin	pg/mg	1.7±0.4	2.0±0.7	1.8±0.3	1.6±0.1	1.78±0.4
MIP-1alpha	ng/mg	0.05±0.02	0.06±0.02	0.05±0.01	0.05±0.00	0.05±0.01
MIP-1beta	pg/mg	26.7±7.6	36.8±13.2	30.9±13.2	27.1±5.2	28.2±5.8
MIP-2	pg/mg	1.7±1.0	1.3±0.3	1.5±0.5	1.8±0.9	1.8±0.5
MIP-3 beta	ng/mg	0.1±0.0	0.2±0.1	0.1±0.0	0.2±0.0	0.2±0.0
MDC	pg/mg	14±5	11±3	12±1	15±5	15±3
MMP-9	pg/mg	16±3	13±6	13±3	14±3	13±3
MCP-1	pg/mg	14±2	17±4	17±4	16±4	20±4
MCP-3	pg/mg	12±3	14±4	13±3	13±3	16±4
MPO	ng/mg	26±12	25±14	15±4	15±5	26±6
Myoglobin	ng/mg	109±26	157±130	138±67	135±54	133±69
OSM	pg/mg	9±2	11±3	9±1	9±0.001	10±2
SAP	pg/mg	0.007±0.002	0.007±0.002	0.006±0.001	0.008±0.001	0.008±0.001
SGOT	μg/mg	N.D.	N.D.	N.D.	N.D.	N.D.
SCF	pg/mg	920±509	404±71	421±143	603±440	531±110
RANTES	pg/mg	0.82±0.51	0.55±0.35	0.56±0.50	0.56±0.31	0.56±0.25
TPO	ng/mg	0.41±0.09	0.39±0.15	0.32±0.11	0.23±0.14	0.27±0.08
TF	ng/mg	0.15±0.03	0.15±0.05	0.15±0.03	0.14±0.03	0.14±0.04

TIMP-1	pg/mg	4±8	3.8±1.2	3.6±0.8	3.5±0.5	3.6±0.6
TNF-alpha	ng/mg	2.4±0.5	2.7±0.7	2.3±0.5	2.1±0.2	2.2±0.5
VCAM-1	ng/mg	4.8±1.0	5.4±1.8	5.2±1.0	5.2±0.9	5.8±0.7
VEGF-A	pg/mg	749±297	759±281	924±317	791±181	689±214
vWF	ng/mg	0.6±0.2	0.5±0.2	0.4±0.1	0.5±0.1	0.5±0.1

Data are mean ± SEM (n= 6 each).
Multiplex immunoassay were peformed using the Luminex LabMAP instruments.
Apo A1 (Apolipoprotein A1), CD (cluster of differentiation), CRP (C Reactive Protein), EGF (Epidermal Growth Factor), FGF-9 (Fibroblast Growth Factor-9), FGF-basic (Fibroblast Growth Factor-basic), GCP-2 (Granulocyte Chemotactic Protein-2), GM-CSF (Granulocyte Macrophage-Colony Stimulating Factor), GST-a (Glutathione S-Transferase alpha), IFN-g (Interferon-gamma), IgA (Immunoglobulin A), IL (Interleukin), IP-10 (Inducible Protein-10), LIF (Leukemia Inhibitory Factor), MCP (Monocyte Chemoattractant Protein), MDC (Macrophage-Derived Chemokine), MIP (Macrophage Inflammatory Protein), MMP-9 (Matrix Metalloproteinase-9), MPO (Myeloperoxidase), OSM (Oncostatin M), RANTES (Regulation Upon Activation, Normal T-Cell Expressed and Secreted), SAP (Serum Amyloid P), SCF (Stem Cell Factor), SGOT (Serum Glutamic-Oxaloacetic Transaminase), TIMP-1 (Tissue Inhibitor of Metalloproteinase Type-1), TNF-a (Tumor Necrosis Factor-alpha), TPO (Thrombopoietin), VCAM-1 (Vascular Cell Adhesion Molecule-1), VEGF (Vascular Endothelial Cell Growth Factor), vWF (von Willebrand Factor). N.D. (Not Detected).

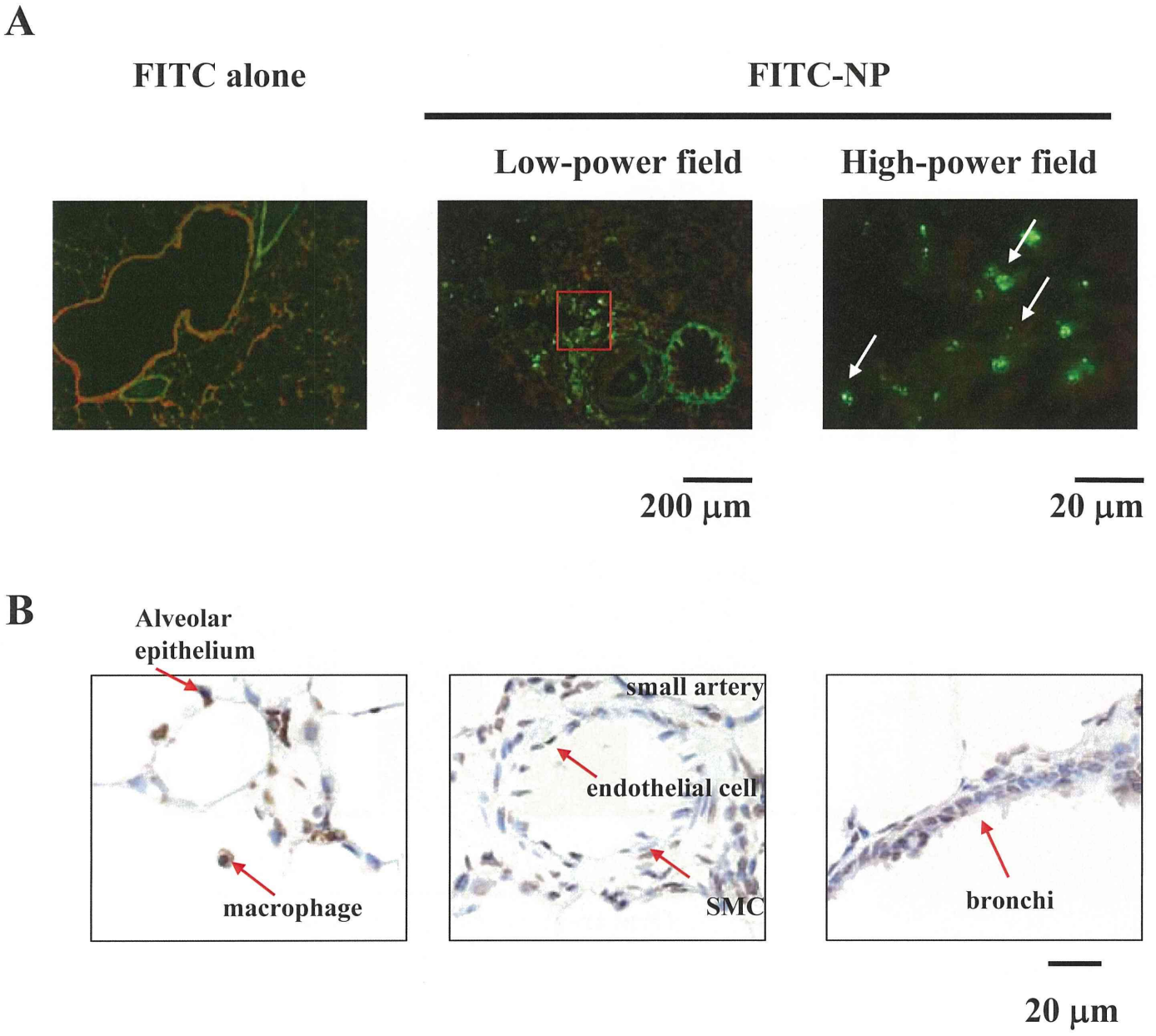

Figure S1. Localization of FITC alone and FITC-NP post-instillation in the rat lung. A, Fluorescent micrographs of cross-sections from lung instillated with FITC alone and FITC-labeled NP on day 3 post-instillation. Nuclei were counterstained with propidium iodide (red). Scale bars: 200 μm and 20 μm.
B, Micrographs of cross-sections stained immunohistochemically against FITC from lung instillated intratracheally with FITC-NP on days 14 post-instillation.

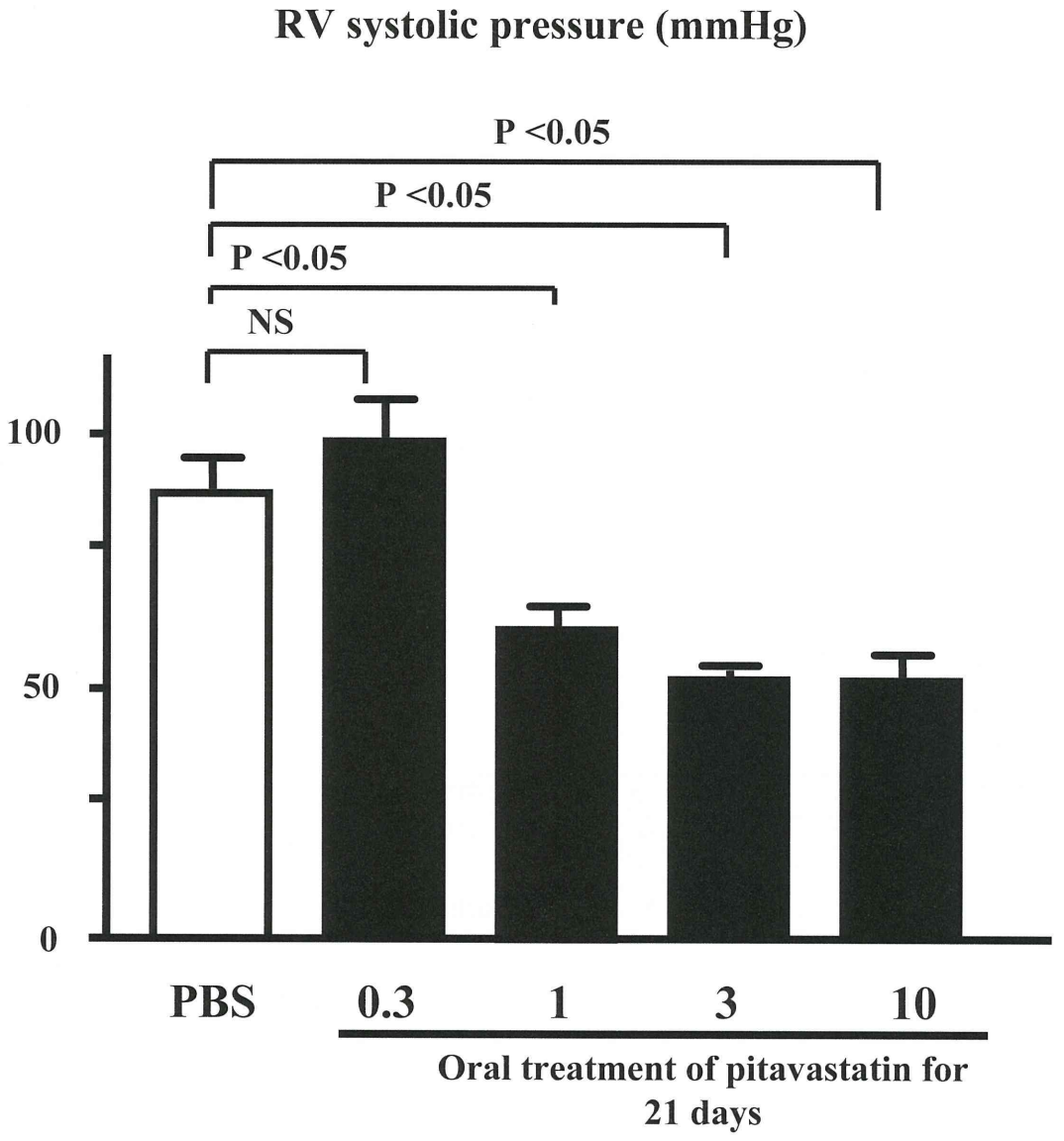

Figure S2. Effects of oral treatment of pitavastatin on right ventricular (RV) systolic pressure 3 weeks after MCT injection. Data are mean ± SEM ($n = 6$ each).

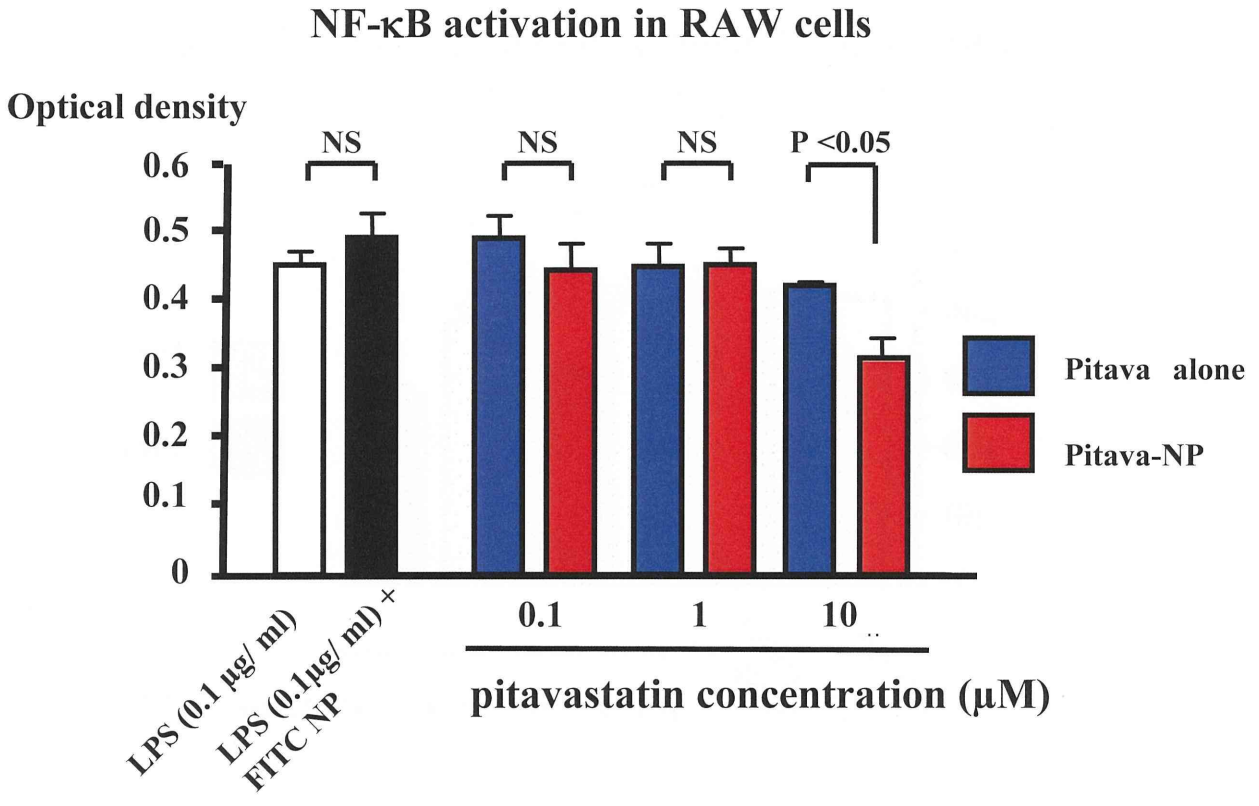

Figure S3 Effect of pitavastatin-NP on NF-κB activation of monocyte cell line (RAW cells)
Effects of pitavastatin-NP on LPS-stimulated activation of NF−κB (ELISA-based DNA binding assay against NF-kB p65 subunit: arbitrary unit). Data are mean ± SEM (n= 6 each).

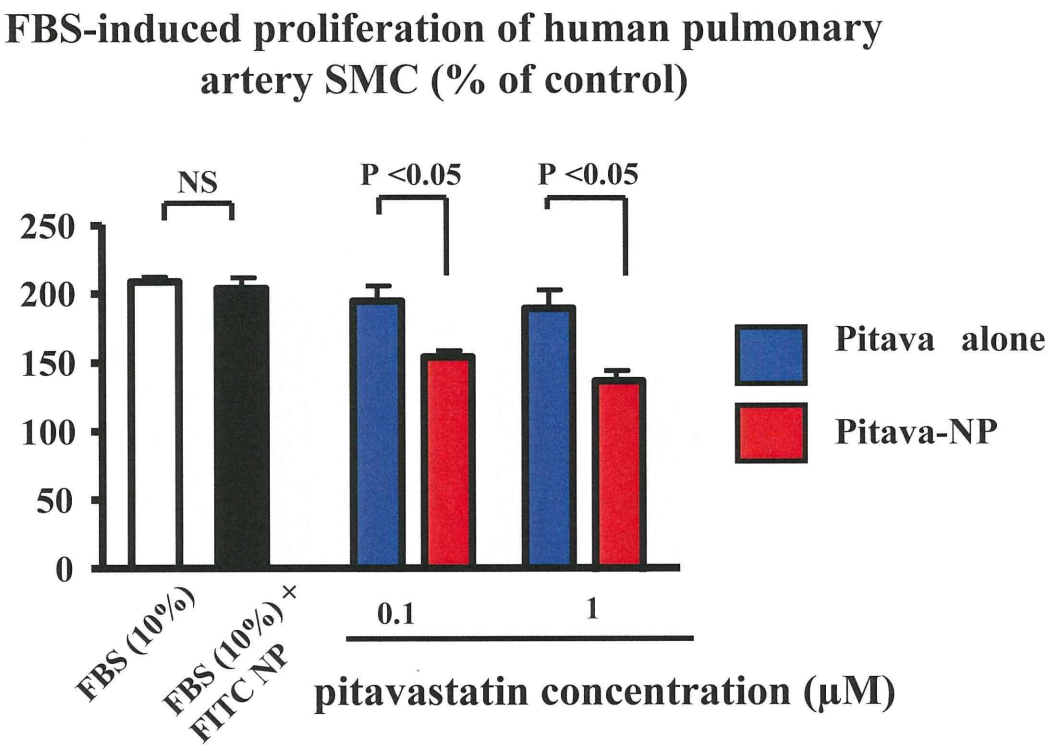

Figure S4. Effects of pitavastatin-NP versus pitavastatin on FBS-induced proliferation of human PASMCs (cell count per well). Data are mean ± SEM (*n* = 6 each).

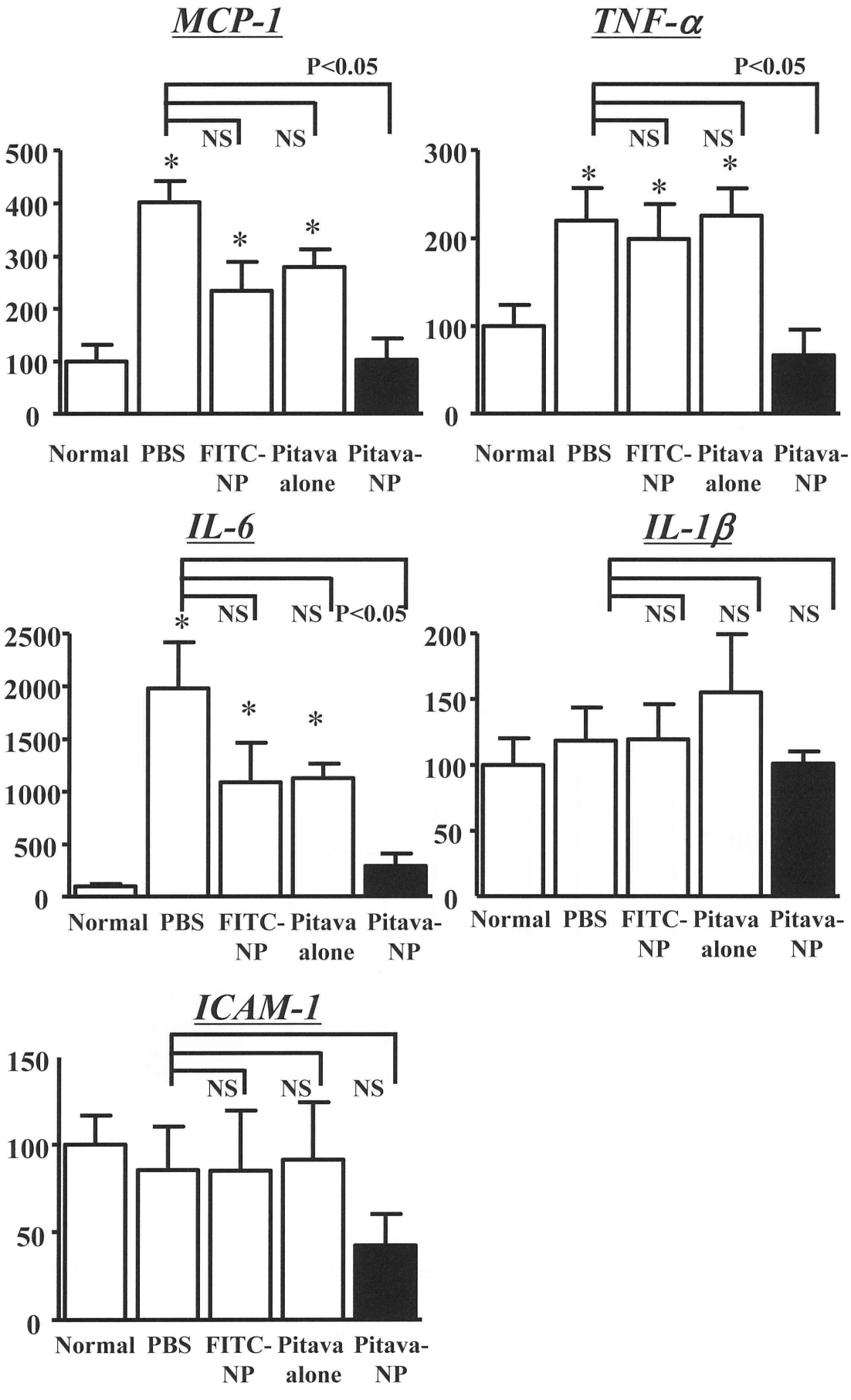

Figure S5. Effects of pitavastatin-NP on mRNA levels of various inflammatory and proliferative factors 21 days after MCT injection (n = 6 each). *$P < 0.05$ versus Normal. Data are mean ±SEM. NS; Not Significant.

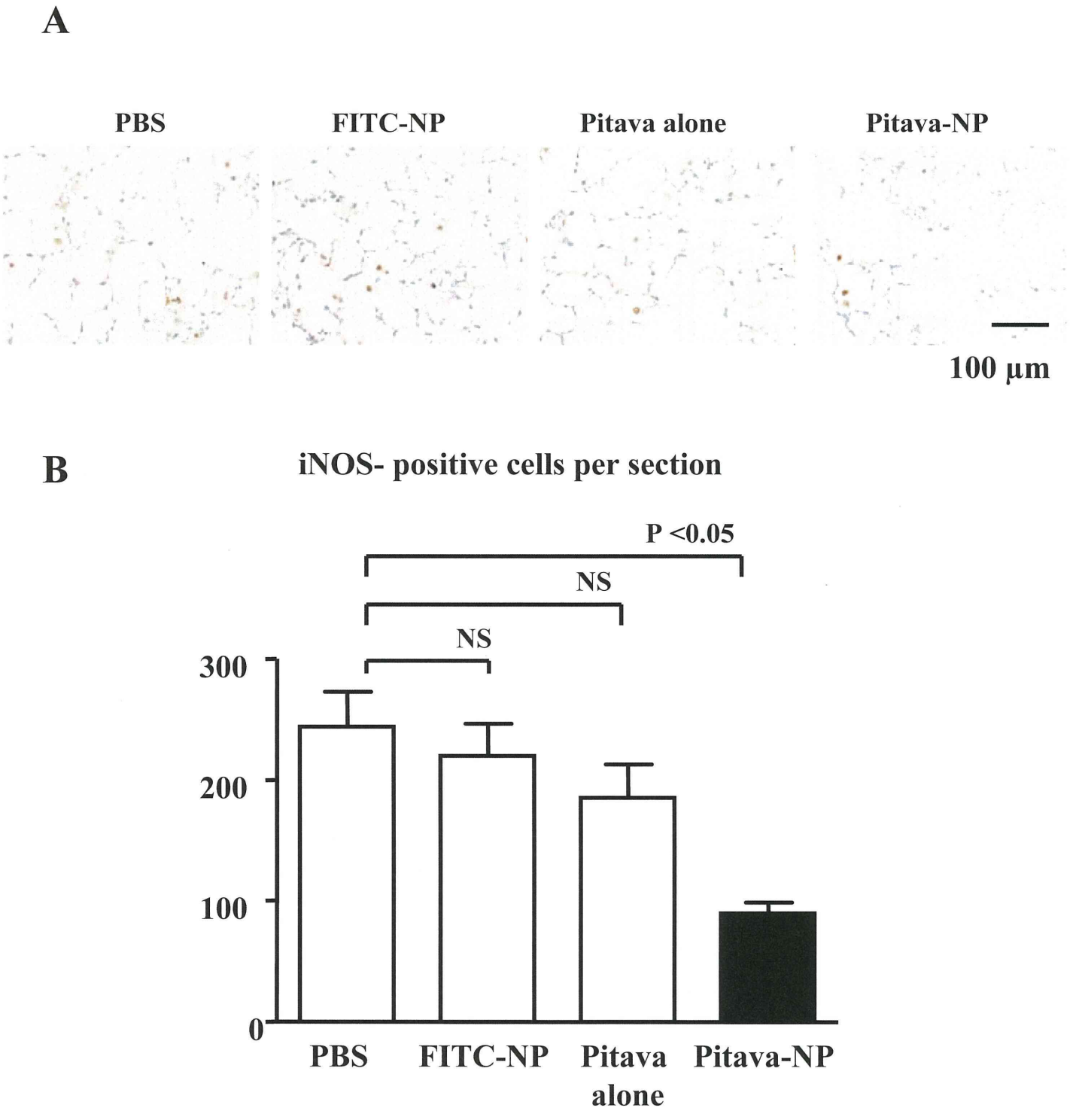

Figure S6. Effects of pitavastatin-NP on iNOS protein expression
A, Representative micrographs of lung tissues stained immunohistochemically for iNOS.
B, Effects of pitavastatin-NP on infiltration of iNOS-positive cells 21 days after MCT injection. Data are mean ±SEM (n = 6 each).

Anti-Inflammatory Gene Therapy for Cardiovascular Disease

Tetsuya Matoba and Kensuke Egashira*

Department of Cardiovascular Medicine, Kyushu University Graduate School of Medical Sciences, Fukuoka, Japan

Abstract: Inflammation in the vascular wall is an essential hallmark during the development of atherosclerosis, for which major leukocytes infiltrated in the lesions are monocytes/macrophages. Therefore, monocyte chemoattractant protein-1 (MCP-1) and its primary receptor CC chemokine receptor 2 (CCR2) are feasible molecular targets for *gene therapy* to inhibit monocyte/macrophage-mediated inflammation in atherogenesis. A mutant MCP-1 that lacks N-terminal 7 amino acids (7ND) has been shown to heterodimerize with native MCP-1, bind to CCR2 and block MCP-1-mediated monocyte chemotaxis by a dominant-negative manner. Gene therapy using intramuscular transfection with plasmid DNA encoding 7ND showed inhibitory effects on atherosclerosis in hypercholesterolemic mice, and neointima formation after vascular injury in animal models. Bare metal stents for coronary intervention were coated with multiple thin layers of biocompatible polymer with 7ND plasmid. The 7ND *gene-eluting stent* inhibited macrophage infiltration surrounding stent struts and in-stent neointima formation in rabbit femoral arteries and cynomolgus monkey iliac arteries. Finally, the authors describe new application of 7ND plasmid encapsulated in polymer nanoparticle (NP) that functions as gene delivery system with unique *in vivo* kinetics. NP-mediated 7ND gene delivery inhibited MCP-1-induced chemotaxis of mouse peritoneal macrophage ex vivo, which may be applicable for the treatment of atherosclerotic cardiovascular disease. In conclusion, anti-inflammatory gene therapy targeting MCP-1/CCR2 signal, with a novel NP-mediated gene delivery system, is a potent therapeutic strategy for the treatment of cardiovascular diseases.

Keywords: ??????????????????????????.

INTRODUCTION

Recent advances in interventional cardiology employing percutaneous coronary intervention (PCI) and other modalities of revascularization have ameliorated symptomatic cardiovascular diseases; however, atherosclerotic cardiovascular disease is still a major cause of death worldwide. In order to improve patients' prognosis, it is needed to develop therapeutics that intervene specific molecular mechanisms underlying disease pathogenesis. Widespread use of transgenic animals has provided various genetic models of human diseases including atherosclerotic cardiovascular disease. Pathological and biochemical analysis in animal models revealed functional consequence of each gene product, which led to basic concept of *gene therapy* to develop new therapeutics for cardiovascular disease. In this manuscript, the authors describe translational application of gene therapy using plasmid DNA for the treatment of atherosclerotic cardiovascular disease, focusing on the gene therapy targeting monocyte-mediated inflammation, and novel nanoparticle-mediated gene delivery system.

ATHEROSCLEROSIS

Recent studies suggest that the inflammatory response plays an important role in the development of atherosclerosis [1]. Chemokines are proinflammatory cytokines, and regulate migration and infiltration of leukocytes into tissues and subsequently cause their activation. During atherogenesis, major leukocytes infiltrated in atherosclerotic lesions are monocytes/macrophages for which monocyte chemoattractant protein-1 (MCP-1) is a primary chemokine that regulates migration and infiltration into the vascular wall. MCP-1 belongs to the CC chemokine subfamily and its primary receptor CC chemokine receptor 2 (CCR2) is dominantly expressed in monocyte and also in vascular endothelial and smooth muscle cells. The importance of MCP-1/CCR2 signaling in athrogenesis is evident from previous studies using genetically-modified mice. Gu *et al.* [2] analyzed atherosclerotic lesions in MCP-1-deficient mice crossed with LDL receptor-deficient mice that develop atherosclerotic lesions in the aorta when fed with high fat diet. Boring *et al.* [3] analyzed CCR2-deficient mice crossed with ApoE-deficient mice that also develop atherosclerotic lesions in the aorta. Both MCP-1/LDL-R double-deficient mice and CCR2/ApoE double-deficient mice developed less atherosclerotic lesions in the aortas. Thus, gene therapy targeting MCP-1/CCR2 signaling is a feasible approach for the treatment of atherosclerotic cardiovascular disease.

We have developed a gene therapy to block MCP-1 activity *in vivo* by using an N-terminal deletion mutant of MCP-1, called 7ND, which lacks the N-terminal amino acid 2 to 8. This mutant MCP-1 has been shown to heterodimerize with native MCP-1, bind to CCR2 and block MCP-1-mediated monocyte chemotaxis by a dominant-negative manner [4] Fig. (**1A**). Plasmid encoding 7ND was constructed by recombinant polymerase chain reaction using a wild-type human MCP-1 cDNA as the template and cloned into BamHI (5') and NotI (3') sites of the pcDNA3 expression vector (Invitrogen) [5] For gene transfer, we injected

*Address correspondence to this author at the Department of Cardiovascular Medicine, Kyushu University Graduate School of Medical Sciences, 3-1-1, Maidashi, Higashi-ku,Fukuoka 812-8582, Japan; Tel: +(81)-92-642-5360; Fax: +(81)-92-642-5374; E-mail: egashira@cardiol.med.kyushu-u.ac.jp

1566-5232/11 $58.00+.00

naked 7ND plasmid vector into skeletal muscles followed by electroporation, and demonstrated that 7ND protein was detectable in the circulating blood over 2 to 4 weeks and blocked monocyte chemotaxis induced by subcutaneous injection of recombinant MCP-1 [6] Fig. (**1B**). Based on these results, we investigated the effect of this gene therapy on the development and progression of atherosclerosis.

ApoE-deficient mice spontaneously develop hypercholesterolemia and atherosclerotic lesions in aortas. We injected with 7ND plasmid into hindlimb muscles of ApoE-deficient mice at 7 to 8 weeks of age, which have not developed apparent atherosclerotic lesions, and evaluate the effect of the transfection on atherogenesis after high cholesterol diet administration. Gene therapy with 7ND plasmid inhibited atherosclerotic lesions without affecting serum lipid concentration [5]. Furthermore, this strategy increased the lesional extracellular matrix content and accordingly, the plaque stability score. These results suggest that MCP-1 is associated with not only atherogenesis but alsoatheromatous plaquevulnerability. We also determined the effect of blockade of MCP-1 on progression of pre-existing atherosclerotic lesions in the aortic root in ApoE KO mice at 20 weeks of age. Gene therapy with 7ND also could limit progression of established lesions [7] In addition, blockade of MCP-1 improved plaque stability (i.e., containing fewer macrophages and lymphocytes, less lipid, more smooth muscle cells and collagen). This strategy decreased expression of CD40 and the CD40 ligand in the atherosclerotic plaque and normalized the increased gene expression of cytokines (MCP-1, RANTES, TNFα, IL-6, IL-1β, and TGF-β1) in the aorta. Suppression of MCP-1 and the other cytokine expression by 7ND gene transfer implies that MCP-1-mediated inflammation causes a vicious cycle to enhance inflammation in the vascular wall by activating lesional monocytes/macrophages. These data suggested that gene therapy with 7ND plasmid is an effective strategy to specifically intervene to MCP-1/CCR2 signaling for the treatment of atherosclerotic cardiovascular disease.

NEOINTIMA FORMATION

Restenosis after PCI consists major part of cardiovascular events in patients of advanced coronary artery disease who underwent PCI even after the introduction of drug-eluting stents (DES). The pathological mechanism of restenosis is undesirable growth of neointima that consists mainly from vascular smooth muscle cells. Drugs on DES inhibit not only vascular smooth muscle cell growth but endothelial cell growth and thus stent re-endothelialization, which causes adverse effects including late stent thrombosis [8]. Therefore, development of new treatment is needed that specifically inhibits undesirable neointima formation. Recent evidence suggests that PCI-induced vascular injury causes an inflammatory response that accelerates recruitment and activation of monocytes through expression of MCP-1 in vascular cells [9, 10]. Inflammation of injured vascular wall results in production of growth factors and other cytokines, which accelerates regrowth of vascular smooth muscle cells causing neointimal hyperplasia. Thus, anti-inflammatory therapy targeting MCP-1-mediated signaling may be an effective approach to treat clinical restenosis.

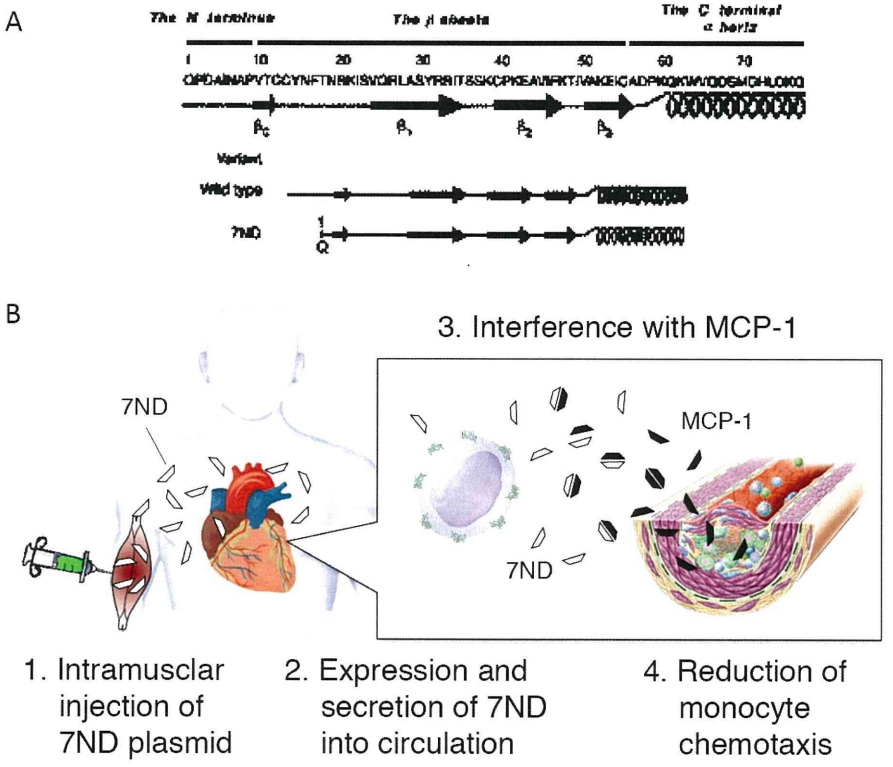

Fig. (1). A, N-terminal deletion mutant of MCP-1 (7ND) lacks the N-terminal amino acids 2 to 8, and acts as a dominant negative inhibitor for MCP-1. **B**, Therapeutic strategy of 7ND gene therapy consists of these 4 steps. 1) Intramusclar injection of 7ND plasmid. 2) Secretion of 7ND into circulation. 3) Interference with MCP-1 in a dominant-negative manner. 4) Reduction of monocyte chemotaxis, which inhibits inflammation in the vascular wall.